Wicking with a yield stress fluid

2009 J. Phys.: Condens. Matter 21 035107

(http://iopscience.iop.org/0953-8984/21/3/035107)

IOP PUBLISHING JOURNAL OF PHYSICS: CONDENSED MATTER

J. Phys.: Condens. Matter **21** (2009) 035107 (6pp) doi:10.1088/0953-8984/21/3/035107

Wicking with a yield stress fluid

V Bertola

School of Engineering and Electronics, University of Edinburgh, King's Buildings, Mayfield Road, Edinburgh EH9 3JL, UK

E-mail: V.Bertola@ed.ac.uk

Received 12 August 2008, in final form 29 October 2008
Published 10 December 2008
Online at stacks.iop.org/JPhysCM/21/035107

Abstract

This work presents an experimental investigation of the flow of a model yield stress fluid (yield stresses between 5 and 21 Pa) driven by capillarity in horizontal glass tubes with diameters ranging from 0.46 to 1.5 mm. It is shown that the liquid penetration stops after typically a few centimeters. The results disagree with a simple model based on the balance between capillary and frictional forces, suggesting that the yield stress fluid constitutive equation may not be valid in the immediate vicinity of the wall. Scaling is proposed with respect to a dimensionless number comparing the yield stress with the capillary pressure.

1. Introduction

The wicking of a Newtonian liquid in a capillary tube (i.e., the ability of the tube to draw the fluid by capillarity) is governed by the well-known Washburn equation [1]. If there are no gravity effects (i.e. the tube is horizontal), the motion is entirely determined by a force balance between capillarity and viscous dissipation, which becomes increasingly larger as the liquid advances. Since the net force acting on the fluid is constant, the mean velocity of the liquid decreases as it progresses. Neglecting inertia, and assuming perfect wetting (zero contact angle), this simple force balance on the cylindrical volume of fluid entered into a horizontal capillary tube of diameter d for a length x yields:

$$\tau_w \pi \, dx = \frac{\pi d^2}{4} \Delta P \tag{1}$$

where $\Delta P = 4\sigma/d$ is the Laplace pressure induced by the surface tension, σ. The mean velocity [2] is $u_m = \sigma d/8\eta x$ (where η is the fluid viscosity), which unlike the shear stress depends on the tube diameter. Because $u_m \to 0$ only for $x \to \infty$, the fluid will always be able reach the end of the tube before stopping.

The global force balance given by equation (1) does not depend on the fluid rheology, so that it is true also for non-Newtonian fluids, and in particular for the so-called viscoplastic or yield stress fluids. Such fluids respond like elastic solids for applied stresses lower than a certain threshold value, which is called the yield stress, and flow only when the yield stress is overcome. A well-known constitutive equation for yield stress fluids is provided by the Herschel–Bulkley model [3], which can be written in the form:

$$\tau = \tau_0 + C\dot{\gamma}^n \tag{2}$$

where $\dot{\gamma} = \mathrm{d}u/\mathrm{d}r$ is the shear rate, τ_0 is the yield stress, and C and n are constants. For $n = 1$ equation (2) reduces to the Bingham model. However, although these models are very popular, their simplicity does not provide always an adequate description of some details of the yield stress fluids phenomenology. To capture these details, constitutive equations based on a more advanced rheophysical modeling are necessary [4].

Practically, this behavior describes many situations, including slurries and suspensions, some polymer solutions, crystallizing lavas, muds and clays, heavy oils, avalanches, cosmetic creams, hair gel, liquid chocolate, and some pastes. Consequently, yield stress fluids have applications in many different fields, ranging from the oil, gas and chemical industries, to food processing, cosmetics and geophysical fluid dynamics. A topic of particular relevance is the duct flow of yield stress fluids [5], which still represents a rich source of problems for both physicists and engineers [6–8].

When a yield stress fluid flows in a horizontal tube under the action of the capillary force only, we might expect from equations (1) and (2) that the meniscus should stop at the critical distance for which the wall shear stress equals the yield value:

$$\bar{x} = \frac{\sigma}{\tau_0}. \tag{3}$$

Since the shear stress is maximum at the wall, this means that $\tau < \tau_0$ everywhere inside the capillary tube, so that the fluid cannot flow anymore. According to equation (3), this critical

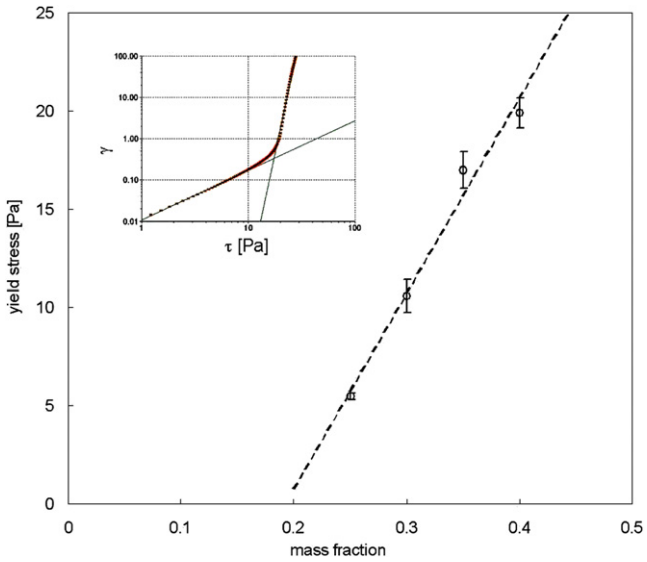

Figure 1. Measured yield stress of the model fluid as a function of the gel concentration. The inset shows the method used to determine the yield point for each fluid sample applying a stress ramp measuring the resulting deformation.

distance should only depend on the physical properties of the fluid, and be independent of the tube diameter.

This work presents experimental results that contradict this argument. It is shown that there is indeed such a finite length of penetration, but this quantity is observed to be much larger than that predicted by equation (3), and to depend strongly on the tube diameter. It is proposed that such behavior could be due to the fact that the constitutive equation of the yield stress fluid may not give an accurate description of the fluid in the immediate vicinity of the wall.

2. Experiments

Model yield stress fluids were prepared using a water-based polymer gel (commercial hairdressing gel). Typically, the composition of these gels includes a blend of water, alcohol, silicones, glycerin, surfactants, and other polymers. In order to change the value of the yield stress in a continuous fashion, the gel was diluted into de-ionized water at different concentrations (six dilutions with weight concentrations of hair-gel equal to 25%, 30%, 32.5%, 35%, 37.5% and 40%, respectively). To avoid foaming, the components were mixed gently and then left at rest overnight to complete diffusion. The fluid homogeneity was controlled by checking that water–gel solutions had a uniform color, which could be verified by visual inspection of the samples.

The yield stress of these model fluids was measured by means of a Haake MARS rotational rheometer, equipped with a plate–plate sensor having a diameter of 35 mm and a gap of 1 mm. Sandpaper was glued on both the rotating an the fixed surface in order to avoid wall slip effects (unlike other yield stress fluid with coarser microstructure, such as foams and emulsions, this is sufficient to eliminate unwanted gap effects in the rheometer) [9]. The yield point of each fluid was

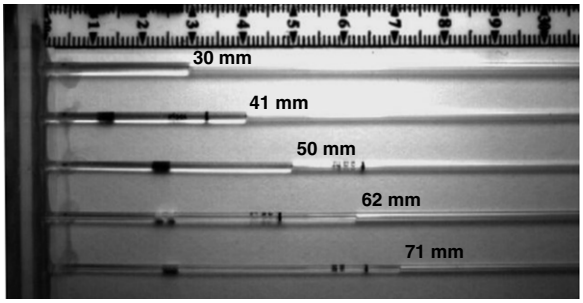

Figure 2. Experimental arrangement of the capillary tubes containing a model yield stress fluid ($\tau_0 = 10.7$ Pa) wicked from the reservoir on the left, 25 min after the beginning of the experiment. The ruler scale is in centimeter.

determined by imposing a stress ramp (100 points in 300 s) on the fluid sample, and measuring the angular displacement of the rotating plate: for small values of the stress, the sample behaves like a solid and has a little deformation; when the stress grows beyond a critical value, the sample starts flowing and therefore the angular displacement of the disk grows indefinitely at a faster rate. The crossover of the two straight lines interpolating the deformation—stress curve in a log–log scale before and after its bending point defined the yield point. The fluid was pre-sheared at a constant shear rate of 50 s^{-1} for 30 s then left at rest for 30 s before each test, to ensure that all samples were in the same conditions. To exclude potential time effects, the same sample was re-tested after 10 min. The measurements are reported in figure 1, which shows that the yield stress is a linear function of the hair-gel mass fraction of the solution; the least-squares best fit gives the following correlation for the yield stress:

$$\tau_0 = 99.4C - 19.1. \tag{4}$$

The equilibrium surface tension of the fluids was measured with a Kruss EasyDyne tensiometer equipped with a De Nouy ring. Since the sensor displacement is imposed, this method is not affected by the yield stress of the fluid: in fact, whatever the concentration of gel, the measured surface tension was 34 ± 2 mN m^{-1}, in good agreement with the value measured for aqueous solutions of polysorbate 20 surfactant above the critical micellar concentration (36 mN m^{-1}) [10]. Because the timescale of the experiments was of the order of hours, dynamic surface tension effects were ignored.

Experiments were carried out using five borosilicate glass tubes 125 mm long, with diameters equal to 0.46, 0.64, 1.02, 1.18 and 1.5 mm, respectively, and glued onto a horizontal support which could be moved using a precision screw. The yield stress fluid was deposited with a laboratory spoon in a small reservoir which was then sealed leaving only a narrow rectangular opening, and put in contact simultaneously with the five capillaries within a very short time (∼10–20 s). Attention was paid to repeat the procedure exactly in the same way, to ensure that experiments had the same initial condition. The arrangement of the tubes during one experiment is shown in figure 2. At the end of each experiment, the fluid was completely replaced and new capillaries were used.

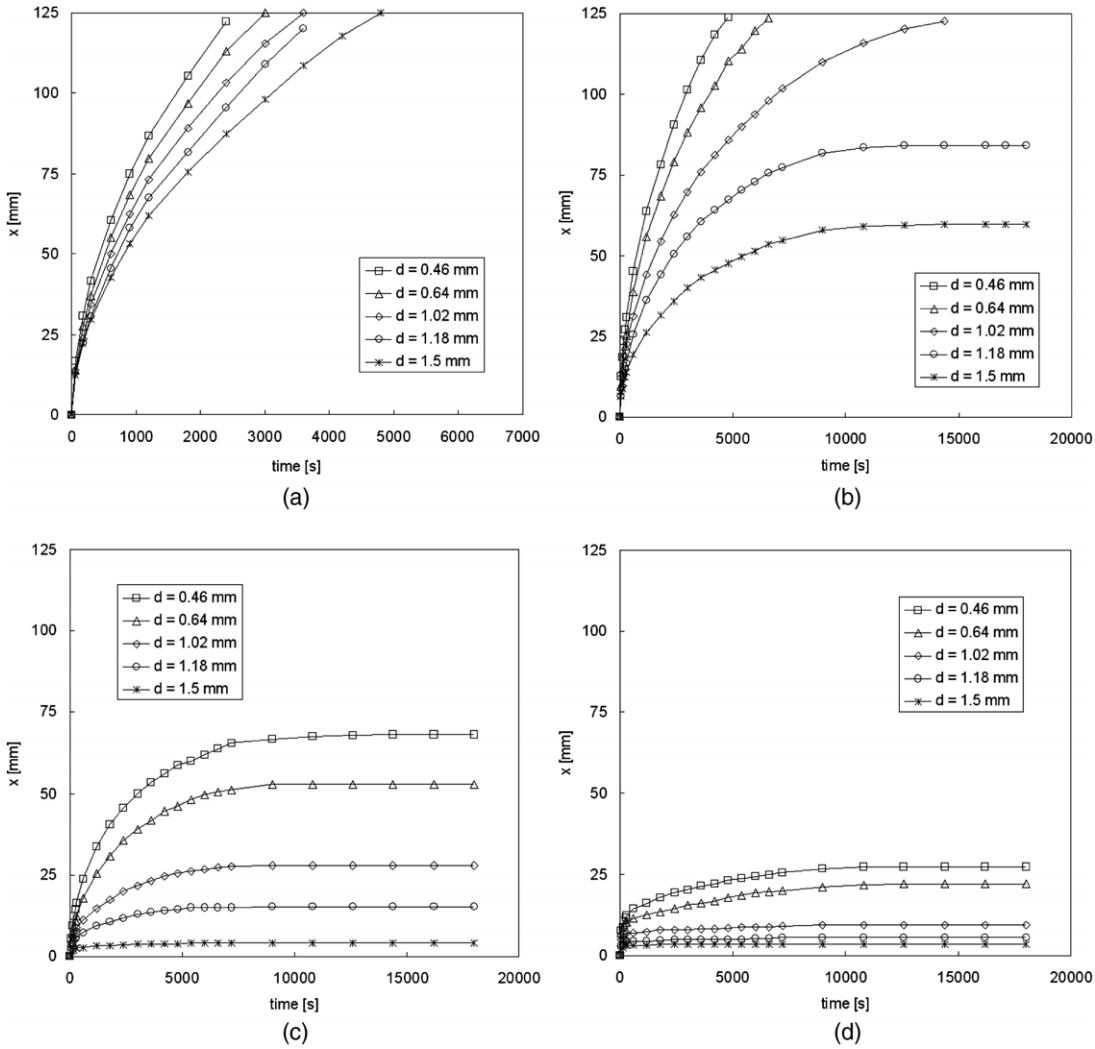

Figure 3. Examples of flow curves obtained in five capillary tubes for different values of the yield stress: (a) $\tau_0 = 5.5$ Pa; (b) $\tau_0 = 10.7$ Pa; (c) $\tau_0 = 15.5$ Pa; (d) $\tau_0 = 20.6$ Pa.

The displacement of the fluid in the capillary tubes was recorded by a CCD camera at a sampling rate of 1 frame min^{-1}, until the fluid stopped moving or reached the end of all the capillaries. Depending on the fluid viscosity and yield stress, the typical duration of each experiment ranged from 1.5 to 6 h (thicker fluids required longer experiments). The digital images captured by a frame grabber were stored on a computer and post-processed to determine the progression of the advancing front of liquid.

3. Results and discussion

The dynamics of the fluid displacement inside the capillary tubes was studied by tracking the position of the meniscus in the capillaries with respect to time. Four examples referred to different values of the model fluid yield stress are shown in figure 3. For low values of the yield stress (figure 3(a)), the fluid reaches the end of the tube in a relatively short time, much like a Newtonian fluid. However, when the yield stress is sufficiently high the flow actually stops before reaching the end of the tube. In all cases, the fluid stops at a distance from the tube inlet that is much larger than the critical length calculated with the simple model outlined above: for example, when the yield stress is 15.5 Pa (figure 3(c)), we expect that the fluid should stop at $\bar{x} = \sigma/\tau_0 = 2.2$ mm, while experiments show values one order of magnitude larger.

Due to the very long timescale of the experiments, the flow may be affected by a thixotropic behavior of the fluid. In particular, because (with the exception of the initial transient in the smaller tubes) the fluid hardly moves, one can reasonably assume that the effect of thixotropy would be an increase of the apparent viscosity. However, the rheometric tests described above show that no systematic changes occur when the sample is re-tested after resting for 10 min. This suggests that when microscopic interactions within the fluid are destroyed by shearing can re-form in a short time (of the order of 1 min).

The summary of all the experiments for which the flow stops before reaching the end of the capillary is reported in figure 4, where the measured wicking length is plotted as a function of the tube diameter for different values of the yield stress: the larger the diameter, the smaller this length

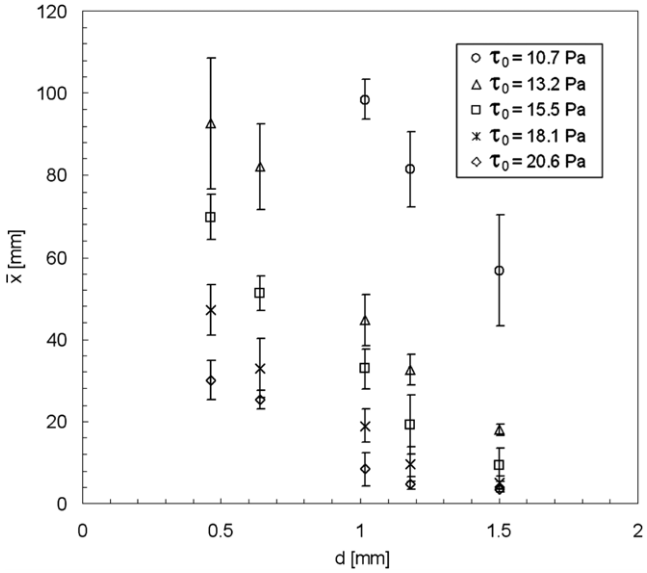

Figure 4. Maximum length of penetration of the yield stress fluid as a function of the tube diameter.

of penetration. This also disagrees with the above argument, where the critical length was expected to depend on the surface tension and the yield stress, but not of the tube diameter.

Taking into account the fluid viscosity, the wicking length must be therefore a function of four quantities (yield stress, surface tension, viscosity and tube diameter), or two dimensionless numbers: the Bingham number, $Bm = \tau_0 D/\eta u$, and the capillary number, $Ca = \eta u/\sigma$. However, the force balance given by equation (1) also defines a dimensionless number which is simply the product of the Bingham number (where the tube diameter has been replaced by the penetration length) and the capillary number, and compares the action of capillarity (or the shear stress at the wall) with the yield point of the fluid:

$$\hat{B} = \frac{\text{yield stress}}{\text{wall shear stress}} = \frac{\tau_0 x}{\sigma}. \tag{5}$$

This number can be used to re-formulate the condition to determine whether the fluid moves in the tube ($\hat{B} < 1$) or not ($\hat{B} \geqslant 1$).

Because the force balance of equation (1) is always true, the simplest explanation for the experimental results shown in figures 3 and 4 is that the fluid does not remain homogeneous under shear flow in the vicinity of the wall, causing a substantial reduction of the effective yield stress. In particular, when a fluid consists of a suspension of particles (including colloids), which is the case of most yield stress fluids, this phenomenon is often caused by a depletion of such particles near the wall [9, 11], not necessarily only at rest but also during flow, because particles are expected to migrate towards regions of less intense shear rates. In the depleted layer of fluid, which has a lower viscosity than the bulk fluid and a thickness of the order of the particles size, the velocity gradient may be very high, so that the velocity profile seems to violate the no-slip boundary condition. It should be noted that a shear-induced yield stress reduction is not necessarily the result of wall depletion, but may be due to other mechanisms: for example, there is evidence that shear flow can lead to structural evolution even in fixed volume fraction suspensions [12].

Apparent wall slip due to depletion has been investigated extensively in rheometric flows, with the purpose of interpreting data affected by wall slip in terms of the effective rheological behavior of the homogeneous fluid [13–15]. It is interesting to observe that in capillaries wall slip also depends on the diameter, and occurs in addition to some bulk flow [14]. More recent measurements of the instantaneous velocity profiles of yield stress fluids confirm that wall slip occurs when the magnitude of the wall shear stress is around the yield point [16].

If the maximum penetration length is calculated using a reduced value for the yield stress in the depleted region near the wall, $\tau_{0,\text{eff}} < \tau_0$, we expect a wicking length $\bar{x} = \sigma/\tau_{0,\text{eff}} > \sigma/\tau_0$, which is compatible with the experimental observations. To prove this scenario, one should be able to relate the onset of wall slip, which can be seen as a failure of the constitutive equation of the fluid [17], to the Bingham-capillary number. In particular, one can check whether a simple one-dimensional theory that describes wall slip and shear banding phenomena in non-Newtonian flows [17, 18] yields the same transition criterion based on the Bingham-capillary number defined by equation (5).

According to the general form of their constitutive relation, the flow equations of non-Newtonian fluids may exhibit a transition from the elliptic to the hyperbolic type [19]. In particular, if the fluid viscosity depends only on the invariants of the velocity gradient tensor (i.e., viscosity is a quantity independent of the coordinate system), the momentum equation for the one-dimensional, steady flow (with one velocity component, w, in the axial direction, z) can be reduced to the form:

$$\frac{\eta(\dot{\gamma})}{\lambda}\left\{\left[\lambda - \left(\frac{\partial w}{\partial x}\right)^2\right]\frac{\partial^2 w}{\partial x^2} + 2\frac{\partial w}{\partial x}\frac{\partial w}{\partial y}\frac{\partial^2 w}{\partial x \partial y} + \left[\lambda - \left(\frac{\partial w}{\partial y}\right)^2\right]\frac{\partial^2 w}{\partial y^2}\right\} = 0 \tag{6}$$

where $\dot{\gamma} = \sqrt{(\frac{\partial w}{\partial x})^2 + (\frac{\partial w}{\partial y})^2}$ is the shear rate, $\eta(\dot{\gamma})$ is the apparent viscosity, and

$$\lambda = -\dot{\gamma}\eta(\dot{\gamma})\frac{\mathrm{d}\dot{\gamma}}{\mathrm{d}\eta}. \tag{7}$$

The parameter λ is related to the rheological properties of the fluid. For $\lambda < 0$ the equation describes a shear-thickening (or dilatant) fluid, while for $\lambda > 0$ the equation describes a shear-thinning fluid.

Equation (6) is formally identical to the momentum equation of the two-dimensional flow of a calorically ideal gas [20]. This can be obtained by replacing the velocity of the non-Newtonian fluid, w, by the velocity potential of the gas, the apparent viscosity by the gas density, and the parameter λ by the square of the speed of sound. Thus, in this analogy, the shear rate of the non-Newtonian fluid corresponds to the velocity of the gas [18].

As it is well known, equation (6) is always elliptic for $\lambda < 0$, while for $\lambda > 0$ it is elliptic if $\dot{\gamma} < \sqrt{\lambda}$ and hyperbolic if $\dot{\gamma} > \sqrt{\lambda}$. Thus, one can define a Mach number for the non-Newtonian flow as $M = \dot{\gamma}/\sqrt{\lambda}$, so that the transition from elliptic to hyperbolic flow occurs at the critical value $M = 1$. At this critical Mach number the viscosity (which in the analogy corresponds to the gas density) and the shear rate (corresponding to the gas velocity) are discontinuous. This model can be thus used to give a simplified description of phenomena like wall slip, but also shear banding and shear-induced phase transitions [21–23].

In the case of yield stress fluids, one can use the common Herschel–Bulkley constitutive model (equation (2)), so that the apparent viscosity is given by $\eta = (\tau_0 + C\dot{\gamma}^n)/\dot{\gamma}$, and the parameter λ can be made explicit. It writes:

$$\lambda = \frac{\dot{\gamma}^2 \tau}{n\tau_0 + (1-n)\,\tau} \tag{8}$$

with a corresponding Mach number:

$$M = \sqrt{1 + n\left(\frac{\tau_0}{\tau} - 1\right)}. \tag{9}$$

The flow equations change from elliptic to hyperbolic for $M = 1$, which occurs for $\tau = \tau_0$: from a physical point of view, this change is represented by a discontinuity of the shear rate and of the apparent viscosity (which in the gas-dynamic analogy correspond to the gas velocity and to the gas density, respectively).

At the tube wall, the shear stress is given by the balance between capillary and viscous forces, i.e. $\tau_w = \sigma/x$, so that:

$$M_w = \sqrt{1 + n\left(\frac{\tau_0 x}{\sigma} - 1\right)}. \tag{10}$$

For $\tau \to \tau_0$ (i.e., $\dot{\gamma} \to 0$), one can use the approximation $n \approx 1$ in the constitutive relationship, which becomes that of an ideal Bingham fluid, and the Mach number at the wall reduces to:

$$M_w = \sqrt{\frac{\tau_0 x}{\sigma}} = \sqrt{\hat{B}}. \tag{11}$$

Thus, the Bingham-capillary number is the square of the Mach number of the non-Newtonian flow evaluated at the tube wall: this means that its critical value ($\hat{B} = 1$) corresponds to a structural change of the fluid near the wall, which causes a reduction of the effective yield stress and apparent wall slip. Consequently, the maximum penetration length is not reached when $\tau_w = \tau_0$ (i.e., when $\hat{B} = 1$), but rather when $\tau_w = \tau_{0,\mathrm{eff}} < \tau_0$ (i.e., when $\hat{B} > 1$), which confirms the conjecture proposed above. At the same time, this analysis suggests that for $\hat{B} > 1$, the flow is no longer of the Hagen–Poiseuille type but may exhibit a discontinuity of the velocity gradient at the tube wall.

Although this argument allows us to understand why the measured penetration length can be greater than expected, it does not capture the dependence on the tube diameter. To investigate the effect of this parameter, one can re-plot the data of figure 4 in dimensionless form with respect to $\hat{B}$, using the tube diameter as characteristic length (in this case, the notation $\hat{B}_d = \tau_0 d/\sigma$ can be used in order to avoid confusion). As shown in figure 5, all the points tend to collapse on a single curve, confirming that the Bingham-capillary number is the main parameter governing this phenomenon.

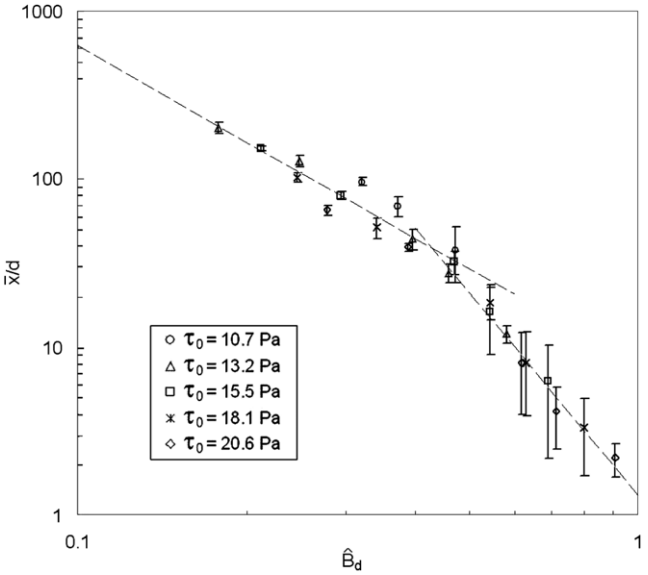

Figure 5. Dimensionless maximum length of penetration of the fluid plotted with respect to the Bingham-capillary number. The dashed lines are the power-law best fits of the experimental data for $\hat{B} < 0.5$ and $\hat{B} > 0.5$, which return $\bar{x}/d = 7.8\hat{B}^{-1.9}$ and $\bar{x}/d = 3.1\hat{B}^{-4.1}$, respectively.

The best fit of the experimental data suggests the following scaling:

$$\begin{aligned} \frac{\bar{x}}{d} &\sim \hat{B}_d^{-2} \qquad \hat{B}_d < 0.5 \\ \frac{\bar{x}}{d} &\sim \hat{B}_d^{-4} \qquad \hat{B}_d > 0.5. \end{aligned} \tag{12}$$

Because when the flow stops $\tau_w = \tau_{0,\mathrm{eff}} = \sigma/\bar{x}$, one can write:

$$\frac{\bar{x}}{d} = \frac{\sigma}{\tau_{0,\mathrm{eff}} d} = \hat{B}_{d,\mathrm{eff}}^{-1} \tag{13}$$

and equation (12) reduces to $\hat{B}_{d,\mathrm{eff}} \sim \hat{B}_d^2$ for $\hat{B}_d < 0.5$ and $\hat{B}_{d,\mathrm{eff}} \sim \hat{B}_d^4$ for $\hat{B}_d > 0.5$.

4. Conclusions

An experimental investigation of the flow of a model yield stress fluid driven by capillarity in tubes of submillimetric diameter shows that wicking stops after typically a few centimeters, in spite of a negligible gravity (tubes were displayed horizontally). The simplest model we can think of, i.e. a balance between capillary and frictional forces, indicates that the fluid should indeed stop flowing when the wall shear stress equals the yield stress. The measured maximum penetration length, however, was found to be much larger than predicted by this simple argument; in addition, it was observed to depend on the tube diameter, which was not expected.

It is suggested that the cause of such behavior is a structural change of the fluid that occurs in the immediate vicinity of the wall (wall depletion), which is known to determine apparent wall slip in many yield stress fluids. Both the onset of slippage (with the associated reduction of the actual yield stress magnitude at the wall) and the dependence of the results on the tube diameter can be captured by introducing a dimensionless number (the product of the Bingham and the Capillary numbers) which expresses the competition between the yield stress and the capillary pressure.

Acknowledgments

The Author is much indebted to David Quéré, who provided the original idea for this study as well as several useful comments. Financial support from the Nuffield Foundation (Grant No. NAL/32355) is gratefully acknowledged.

References

[1] Washburn E W 1921 The dynamics of capillary flow *Phys. Rev.* 273–83
[2] Tritton D J 1988 *Physical Fluid Dynamics* 2nd edn (Oxford: Oxford University Press)
[3] Bird R B, Gance D and Yarusso B J 1982 The rheology and flow of viscoplastic materials *Rev. Chem. Eng.* **1** 1–70
[4] Coussot P 2007 Rheophysics of pastes: a review of microscopic modelling approaches *Soft Matter* **3** 528–40
[5] Skelland A H 1967 *Non-Newtonian Flow and Heat Transfer* (New York: Wiley)
[6] Daprà I and Scarpi G 2004 Start-up of channel-flow of a Bingham fluid initially at rest *Rendiconti Lincei-Matematica e Applicazioni* s.9 **15** 125–35
[7] Engin T, Dogruer U, Evrensel C, Heavin S and Gordaninejad F 2004 Effect of wall roughness on laminar flow of Bingham plastic fluids through microtubes *Trans. ASME, J. Fluids Eng.* **126** 880–3
[8] Nouar C 2005 Thermal convection for a thermodependent yield stress fluid in axisymmetrical horizontal duct *Int. J. Heat Mass Transfer* **48** 5520–35
[9] Barnes H A 1995 A review of the slip (wall depletion) of polymer solutions, emulsions and particle suspensions in viscometers: its cause, character, and cure *J. Non-Newton. Fluid Mech.* **56** 221–51
[10] Mittal K L 1972 Determination of CMC of polysorbate 20 in aqueous solution by surface tension method *J. Pharm. Sci.* **61** 1334–5
[11] Kok P J A H, Kazarian S G, Briscoe B J and Lawrence C J 2004 Effects of particle size on near-wall depletion in mono-dispersed colloidal suspensions *J. Colloid Interface Sci.* **280** 511–7
[12] Varadan P and Solomon M J 2001 Shear-induced microstructural evolution of a thermoreversible colloidal gel *Langmuir* **17** 2918–29
[13] Mooney M 1931 Explicit formulas for slip and fluidity *J. Rheol.* **2** 210–22
[14] Jastrzebski Z D 1967 Entrance effects and wall effects in an extrusion rheometer during the flow of concentrated suspensions *Ind. Eng. Chem. Fundam.* **6** 445–53
[15] Yoshimura A and Prud'homme R K 1988 Wall slip corrections for Couette and parallel disk viscometers *J. Rheol.* **32** 53–67
[16] Bertola V, Bertrand F, Tabuteau H, Bonn D and Coussot P 2003 Wall slip and yielding in pasty materials *J. Rheol.* **47** 1211–26
[17] Bertola V and Cafaro E 2007 Analytical solution for the Hagen-Poiseuille flow of a hard sphere gas with nonlinear shear viscosity *J. Stat. Mech.* P06017
[18] Bertola V and Cafaro E 2003 Analogy between pipe flow of non-Newtonian fluids and 2D compressible flow *J. Non-Newton. Fluid Mech.* **109** 1–12
[19] Joseph D D 1990 *Fluid Dynamics of Viscoelastic Liquids* (New York: Springer)
[20] Emanuel G 1986 *Gasdynamics: Theory and Applications* (*AIAA Education Series*) (New York: AIAA)
[21] Olmsted P D 1999 Dynamics and flow-induced phase separation in polymeric fluids *Curr. Opin. Colloid Interface Sci.* **4** 95–100
[22] Vermant J and Solomon M J 2005 Flow-induced structure in colloidal suspensions *J. Phys.: Condens. Matter* **17** R187–216
[23] Fischer E and Callaghan P T 2001 Shear banding and the isotropic-to-nematic transition in wormlike micelles *Phys. Rev.* E **64** 011501-1